p53 Contributes to Differentiating Gene Expression Following Exposure to Acetaminophen and Its Less Hepatotoxic Regioisomer Both *In Vitro* and *In Vivo*

Brendan D. Stamper[1], Michael L. Garcia[1], Duy Q. Nguyen[1], Richard P. Beyer[2], Theo K. Bammler[2], Frederico M. Farin[2], Terrance J. Kavanagh[2] and Sidney D. Nelson[3]

[1]School of Pharmacy, Pacific University, Hillsboro, OR, USA. [2]Department of Environmental and Occupational Health Sciences. [3]Department of Medicinal Chemistry, University Of Washington, Seattle, WA, USA.

ABSTRACT: The goal of the present study was to compare hepatic toxicogenomic signatures across *in vitro* and *in vivo* mouse models following exposure to acetaminophen (APAP) or its relatively nontoxic regioisomer 3′-hydroxyacetanilide (AMAP). Two different Affymetrix microarray platforms and one Agilent Oligonucleotide microarray were utilized. APAP and AMAP treatments resulted in significant and large changes in gene expression that were quite disparate, and likely related to their different toxicologic profiles. Ten transcripts, all of which have been implicated in p53 signaling, were identified as differentially regulated at all time-points following APAP and AMAP treatments across multiple microarray platforms. Protein-level quantification of p53 activity aligned with results from the transcriptomic analysis, thus supporting the implicated mechanism of APAP-induced toxicity. Therefore, the results of this study provide good evidence that APAP-induced p53 phosphorylation and an altered p53-driven transcriptional response are fundamental steps in APAP-induced toxicity.

KEYWORDS: acetaminophen, AMAP, microarray, p53, TAMH, toxicogenomics

Introduction

Acetaminophen (APAP, paracetamol, acetyl-*p*-aminophenol) is a widely used analgesic and antipyretic. While considered safe at recommended doses, APAP overdose cases are quite common and lead to over 50,000 emergency room visits annually in the United States alone.[1,2] The toxicity associated with APAP overdose cases is related to cytochrome P450-mediated bioactivation of APAP into *N*-acetyl-*p*-quinoneimine (NAPQI),[3] which can form APAP adducts on proteins leading to toxicity. Although a great deal is understood regarding the mechanisms underlying the pathophysiology of APAP-induced liver injury, the most important pathways involved continue to be debated.

Toxicogenomics is a field in which global changes in gene expression can be assessed quickly and efficiently to generate hypotheses and relate changes in expression to toxicity.[4] Early experiments in the field of toxicogenomics found microarray technology to be a sensitive and powerful tool able to not only correlate gene expression with histopathology[5] but also generate highly reproducible results.[6] While it has been demonstrated that microarray data generated from multiple sites can maintain a good degree of consistency and reproducibility when utilizing the same platform,[7] consistent and reproducible

data from labs using the same samples and different platforms can be difficult to obtain.[8] In addition to platform variation, the type of system, variability in lab techniques, and unique methods for sample preparation make relating different genomic studies quite difficult. Therefore, consistent microarray results obtained from different laboratories using the same platforms should be considered quite robust.

A number of toxicogenomic studies have been performed on APAP-treated samples to identify transcriptomic hallmarks that may be related to APAP-induced toxicity.[9–14] In order to obtain a clearer picture of the transcriptomic changes occurring during APAP-induced toxicity, structure–toxicity relationships can be utilized to differentiate between cellular changes related to the pharmacology of APAP and those related to toxicity. 3′-Hydroxyacetanilide (AMAP, acetyl-*m*-aminophenol) is a relatively nontoxic positional isomer of APAP that has analgesic and antipyretic activity similar to APAP in mice,[15] and therefore can be used to discriminate between APAP-induced changes related to the pharmacologic and therapeutic activity of hydroxyacetanilides and APAP-induced changes related to toxicity. This comparative toxicogenomic approach has been utilized in a handful of previous studies attempting to identify genes associated

with APAP-induced toxicity rather than its pharmacologic effects.[7,16,17]

One important consideration when comparing drug-induced gene expression profiles, especially with compounds as structurally similar as APAP and AMAP, is that while each regioisomer will likely produce unique expression, it may be difficult to distinguish toxic and pharmacologic mechanisms due to significant overlap. To overcome this hurdle, it was imperative to collect as many transcriptomes as possible across multiple concentrations and time-points to differentiate between effects associated with various treatment conditions.[18] In the present study, three microarray experiments were compared in two model systems across four time-points using three different microarray platforms to identify robust transcript expression responsible for the different toxicologic outcomes associated with APAP and AMAP treatment. More specifically, gene expression was compared between transforming growth factor alpha 1 (TGF-α)-transfected mouse hepatocytes (TAMH cells) using two Affymetrix platforms (Mouse Genome 430 2.0 and Mouse Gene 1.0 ST arrays)[17] and C57BL/6 mice on an Agilent Mouse Oligonucleotide array.[7]

Despite the diversity of cell models and microarray platforms employed in this study, the detection of common gene expression patterns was observed. In general, APAP treatment altered gene expression to a greater extent than AMAP treatment. Furthermore, significant changes in gene expression, likely related to pharmacological effects, were relatively well conserved between the regioisomers *in vitro*, but not *in vivo*. However, gene expression changes that were significant and large were much less conserved between APAP and AMAP both *in vitro* and *in vivo* and were likely related to toxicological differences. The most conspicuous gene targets identified by these experiments related to APAP-induced toxicity included *Atf3, Btg2, Cdkn1a, Egr1, Gdf15, Jun, Lif, Mdm2, Myd116*, and *Plk3*. Interestingly, 9 out of 10 of these transcripts (ie, all except *Jun*) have been shown to positively regulate the activity of p53, thus implicating a role for p53 in the toxicogenomic response to APAP-induced hepatotoxicity.

The tumor suppressor p53 has been extensively studied for over 30 years.[19] Its activity is regulated via reversible posttranslational modifications, which include phosphorylation, acetylation, ubiquitination, and neddylation.[20] These modifications occur in response to numerous stimuli such as cell stress and DNA damage, which are well-established events in APAP overdose situations.[21] Previous studies have demonstrated increased phosphorylation at the N-terminus of p53 following APAP-induced oxidative DNA damage (eg, serine-15, serine-20, and serine-37).[22,23] These results were validated in the present study, in addition to the observation that APAP treatment led to increased phosphorylation at serine-329 in the C-terminal region of p53 compared to AMAP treatment and vehicle-treated controls. Increased p53 phosphorylation at serine-392 in response to DNA damage

following UV exposure has been established.[24–26] However, to our knowledge, this is the first published evidence of APAP-induced p53 phosphorylation at this site.

Materials and Methods

Materials. Acetaminophen, 3′-hydroxyacetanilide, glycine, dexamethasone, nicotinamide, ethanol, and soybean trypsin inhibitor were obtained from Sigma-Aldrich. Gentamicin, trypsin, Dulbecco's Modified Eagle's Medium/Ham's F12 (1:1), Dulbecco's PBS (DPBS), Hank's balanced salt solution, and Trizol reagent were purchased from Invitrogen. ITS premix was obtained from BD Bioscience. Tissue culture plates, dishes, and scrapers were purchased from Fisher. Chloroform was purchased from MP Biomedicals. Needles (22G) were purchased from Becton, Dickinson and Company. Nuclease-free water and RNeasy kits were purchased from Qiagen. All reagents used in the processing of total RNA for Affymetrix microarrays were supplied in the One-Cycle Target Labeling and Control Reagents Kit from Affymetrix. The reagents used for processing RNA for Agilent arrays were purchased from Agilent Technologies. All antibodies for immunoblotting were purchased through Cell Signaling Technology.

Cell culture. TAMH cells (passages between 25 and 35) were grown in serum-free Dulbecco's Modified Eagle's/Ham's F12 (1:1) medium supplemented with (final concentrations) 100 nM dexamethasone, 10 nM nicotinamide, 0.1% (v/v) gentamicin, and an ITS premix containing insulin (5 ng/mL), transferrin (5 ng/mL), and selenium (5 ng/mL). Cells were grown at 37 °C in a humidified incubator with 5% CO_2 and 95% air, and passaged as previously described.[17]

In vitro **RNA isolation.** RNA was isolated from TAMH cells dosed with 2 mM APAP, 2 mM AMAP, or control culture media for 2, 6, or 24 hours. For each treatment, cells were grown to confluence in two 150 mm² tissue culture dishes and dosed. At the end of each treatment, cells were harvested using a rubber scraper and collected by centrifugation. Following an ice-cold Dulbecco's phosphate buffered saline (DPBS) wash step, Trizol reagent was added directly to the cell dish. Once vortexed, the cell suspension was passed through a 22G needle multiple times to ensure complete cell lysis. Following the addition of a chloroform solution and a centrifugation step, the aqueous phase of the sample mixture was isolated and dissolved in 70% ethanol. The resulting mixture was loaded onto a Qiagen RNeasy column, and purified total RNAs were eluted according to the manufacturer's protocol.

Affymetrix mouse genome 430 2.0 arrays. RNA integrity was assessed using the Agilent 2100 Bioanalyzer, and only samples passing quality control were further processed. The manufacturer's protocol was then followed for the determination of gene expression data using nine Affymetrix Mouse Genome 430 2.0 arrays (*n* = 1 per group). Included in these methods are first and second strand cDNA synthesis, double-stranded cDNA purification, cRNA synthesis, biotin-labeled

cRNA quantification, and cRNA fragmentation followed by subsequent hybridization. Following hybridization and washing, the Affymetrix arrays were scanned with an Affymetrix GeneChip 3000 scanner. Image generation and feature extraction were performed using the Affymetrix AGCC Software. Only data from arrays that passed the manufacturer's quality specifications were used for further analysis. It is worth mentioning that all tables containing expression data convey gene changes as log2 fold changes. All microarray data derived from Affymetrix Mouse Genome 430 2.0 arrays used in this study have been deposited in the Gene Expression Omnibus Database under accession number GSE56576 (http://www.ncbi.nlm.nih.gov/geo/).

Affymetrix mouse gene 1.0 ST arrays. RNA integrity was assessed using the Agilent 2100 Bioanalyzer, and only samples passing quality control were further processed. The manufacturer's protocol was then followed for the determination of gene expression data using 28 Affymetrix Mouse Gene 1.0 ST arrays ($n = 3$ per group). Included in these methods are first and second strand cDNA synthesis, double-stranded cDNA purification, cRNA synthesis, biotin-labeled cRNA quantification, and cRNA fragmentation followed by subsequent hybridization. Following hybridization and washing, Affymetrix arrays were scanned with an Affymetrix GeneChip 3000 scanner. Image generation and feature extraction were performed using the Affymetrix AGCC Software. Only data from arrays that passed the manufacturer's quality specifications were used for further analysis. All microarray data derived from Affymetrix Mouse Gene 1.0 ST arrays used in this study have been deposited in the Gene Expression Omnibus Database under accession number GSE18614 (http://www.ncbi.nlm.nih.gov/geo/).

Agilent mouse oligonucleotide arrays. Details regarding animal treatments, RNA isolation, and microarray hybridizations can be found in the original publication by the Toxicogenomics Research Consortium.[7] All animal studies for this project were approved by each Institution's respective Animal Care and Use Committee. Briefly, randomly assigned C57BL/6 J mice were dosed with 10 mL/kg body weight of vehicle (methylcellulose, 0.5% wt/vol), AMAP (300 mg/kg), or APAP (300 mg/kg). Mice were euthanized at 6, 12, or 24 hours after treatment. Total RNA was isolated from liver samples (left lateral lobe) using Qiagen RNeasy mini kits according to the manufacturer's protocol. Total RNA from individual mouse liver samples was amplified and labeled with a fluorescent dye (Cy3), whereas a common reference of pooled C57BL/6 J liver mRNA was amplified and labeled with Cy5 using Agilent Technologies Low RNA Input Linear Amplification Labeling Kit following the manufacturer's protocol. Equal amounts of Cy3 and Cy5-labeled cRNA were hybridized to an Agilent Mouse Oligonucleotide Microarray (~21,000 features, catalog # G4121) and scanned using an Agilent G2565BA scanner. Raw microarray data were processed and analyzed with tools in the Bioconductor[27]

software package. This dataset (raw and normalized data files) is publicly available from *cebs.niehs.nih.gov* (accession number 009–00001–0010–000–1).

Statistical analysis. From the normalized data, genes with evidence for statistically significant differential expression were identified using the limma package[28] in Bioconductor.[27] The *P*-values were calculated with a modified *t*-test in conjunction with an empirical Bayes method to moderate the standard errors of the estimated log-fold changes. The *P*-values were adjusted for multiplicity using Bioconductor's implementation of the Benjamini–Hochberg method,[29] which allows selecting statistically significant genes while controlling the estimated false discovery rate.

Immunoblotting and quantification. TAMH cells were dosed with 2 mM of APAP, 2 mM of AMAP, or control media for 2 and 6 hours (as described previously). Subsequent to treatment, cells were harvested by using a rubber scraper. Pierce BCA protein assay kit was then utilized to determine the protein concentration of each sample. BCA quantification was performed via spectrophotometry using the Biotek Synergy 2 Multi-Mode Microplate Reader. Normalization using total protein analysis, in place of loading controls such as β-actin and β-tubulin, is a well-established model to determine whether equivalent protein loading is achieved.[30] Based on concentration data from the bicinchoninic acid (BCA) assay, appropriate volumes of $1 \times$ SDS sample buffer were added to each sample to ensure that 50 µg of protein was loaded per well. Samples were then heated at 97.5 °C for five minutes followed by centrifugation at 2000 rpm for five minutes. Fifty micrograms of protein per well was loaded on Bio-Rad Any kD Mini-PROTEAN TGX gels, and electrophoresis was performed at 150 V for 45 minutes using the Bio-Rad Mini-PROTEAN Tetra Cell system. Upon completion, transfer to poly(vinylidene fluoride) PVDF membrane was performed using the Bio-Rad TransBlot SD semi-dry transfer cell at 15 V for 60 minutes. Each membrane was blocked in 20 mL of blocking buffer (5% BSA, pH 8) at room temperature with gentle shaking for 60 minutes. Primary antibodies were diluted in 5% BSA blocking buffer (1:1000 for phospho-p53 S15 and 1:500 for phospho-p53 S392, and 1:1000 for total p53) and incubated with membranes overnight at 4 °C. Membranes were then treated with their respective horseradish peroxide (HRP)-linked secondary antibodies (1:1500 for anti-mouse IgG, and 1:1000 for anti-rabbit IgG) at room temperature for 60 minutes and exposed to LumiGLO chemiluminescent substrate (Cell Signaling Technologies) with gentle agitation for one minute. Detection was visualized after 30 minutes on green X-Ray film (Phenix Research Products). Films were then subjected to densitometric analysis via the software ImageJ (developed by Wayne Rashband, National Institutes of Health, Bethesda). All antibodies were purchased from Cell Signaling Technologies, which included phospho-p53 S15 (#9284), phospho-p53 S392 (#9281), p53 (#2524), anti-mouse IgG (#7076), and anti-rabbit IgG (#7074).

Results

Comparison of APAP- and AMAP-induced transcriptomic changes relative to vehicle control using Affymetrix mouse genome 430 2.0 arrays. In order to identify transcriptional changes that may be responsible for the observed differences in toxicity, an exploratory microarray experiment was performed with RNA isolated from TGF-α TAMH exposed to 2 mM APAP or 2 mM AMAP. Microarray analysis was then performed on one sample per treatment condition using Affymetrix Mouse Genome 430 2.0 arrays. The expression of 5753 transcripts changed more than twofold relative to the vehicle control in at least one of the three time-points (2, 6, or 24 hours) following either APAP or AMAP treatment. One-dimensional clustering of these 5753 transcripts revealed that the isomers induced very similar large changes in gene expression as evidenced by the fact that samples clustered based on time-point rather than by drug (Supplementary Fig. 1). Unfortunately, statistical significance related to these differences could not be determined due to the lack of replicates at each time-point ($n = 1$ per treatment condition). Owing to the nature of the array as an exploratory comparison, no validation of transcriptomic changes through quantitative polymerase chain reaction (qPCR) or subsequent western analysis was performed based solely on these results.

Follow-up comparison of APAP- and AMAP-induced transcriptomic changes relative to the vehicle control using affymetrix mouse gene 1.0 ST arrays. A second comparative toxicogenomic experiment was performed in triplicate on the Affymetrix Mouse Gene 1.0 ST platform for two reasons. First, it was important to assign significance to transcriptional changes of interest for the exploratory Affymetrix Mouse Genome 430 2.0 experiments; and second, it was anticipated that consistent changes in gene expression across different Affymetrix platforms would minimize the potential for platform bias. To this end, RNA was isolated from TAMH cells following 2, 6, or 24 hour exposure to 2 mM APAP or

2 mM AMAP. Samples were then processed and analyzed by microarray. A total of 9121 transcripts were found to have expression that was significantly altered ($P < 0.05$) in at least one of the time-points/treatments relative to controls. In fact, APAP and AMAP treatment induced similar transcriptomic changes, as illustrated by the fact that these changes clustered more closely with respect to dosing period rather than with drug treatment (Fig. 1A). However, when a dendrogram was generated for the 524 gene expression changes found to be both significant ($P < 0.05$) and different by at least 50% from controls (ie, |fold change| >1.5) in at least one of the time-points/treatments relative to controls, gene expression patterns clustered according to drug treatment rather than to dosing period (Fig. 1B). This suggests that overall gene expression changes following APAP and AMAP treatment is quite similar *in vitro*, but that the regioisomers have very different effects on a specific subset of genes in which large changes in expression were observed.

***In vivo* comparison of APAP- and AMAP-induced transcriptomic changes in liver relative to the vehicle control using agilent mouse oligonucleotide arrays.** A third comparative toxicogenomic experiment previously published by the Toxicogenomics Research Consortium[7] was analyzed to 1) identify *in vivo* transcriptomic changes in C57BL/6J mouse liver that were predicted by the TAMH *in vitro* model, and 2) to verify that these consistent gene expression changes were platform-independent (Affymetrix platforms vs Agilent). Mice were dosed with 300 mg/kg APAP or AMAP for 6, 12, or 24 hours, an adequate and validated dose for toxicity studies involving APAP in the C57BL/6 model.[11,13,31] A total of 14,161 transcripts were found to have expression that was significantly altered ($P < 0.05$) in at least one of the time-points/treatments relative to controls. However, unlike the TAMH *in vitro* model, significant gene expression changes clustered more closely with respect to drug treatment rather than dosing time (Fig. 2A). This clustering pattern related to drug

Figure 1. Clustering of significant transcriptomic changes *in vitro* following APAP or AMAP treatment compared to control. TAMH cells were treated with 2 mM APAP or AMAP for 2, 6, or 24 hours and gene expression was analyzed using Affymetrix Mouse Gene 1.0 ST arrays ($n = 3$). (**A**) Dendrogram relating gene expression patterns for the 9121 genes that underwent significant changes in expression in at least one of the time-points/treatments compared to controls ($P < 0.05$). (**B**) Dendrogram relating gene expression patterns for the 524 genes that underwent significant and large changes in expression in at least one of the time-points/treatments compared to controls (|log2| >1.5, $P < 0.05$).
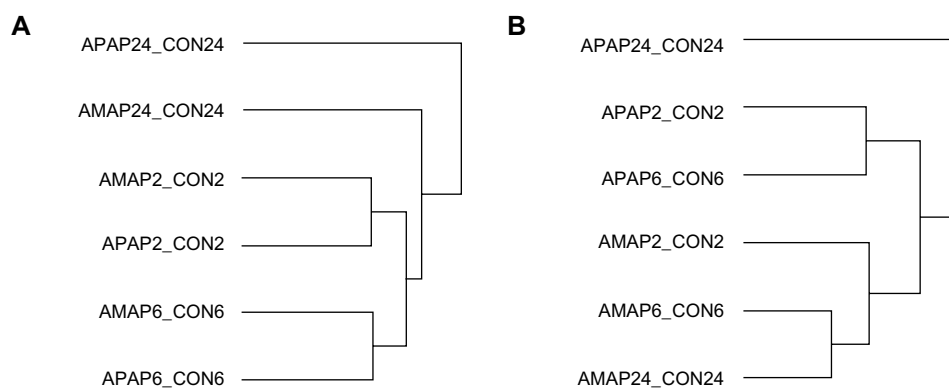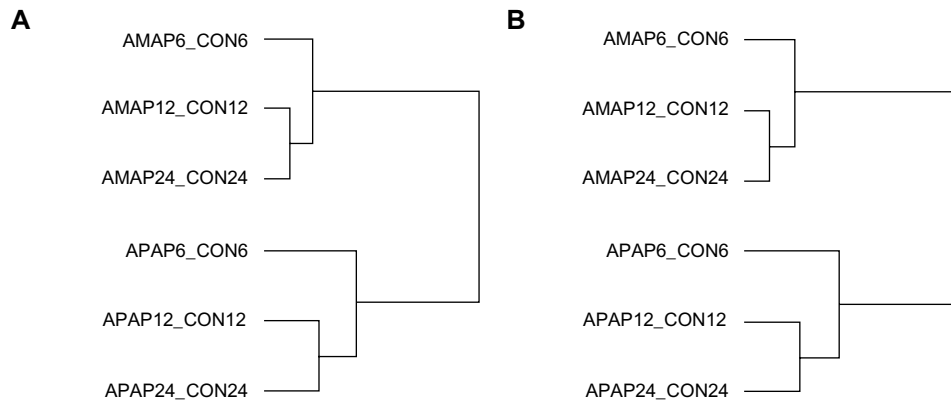
Figure 2. Clustering of significant transcriptomic changes *in vivo* following APAP or AMAP treatment compared to control. C57BL/6J mice were dosed with 300 mg/kg APAP or AMAP for 6, 12, or 24 hours and analyzed using Agilent Mouse Oligonucleotide arrays (*n* = 23–28).[7] (**A**) Dendrogram relating gene expression patterns for the 14,161 genes that underwent significant changes in expression in at least one of the time-points/treatments compared to controls (*P* < 0.05). (**B**) Dendrogram relating gene expression patterns for the 931 genes that underwent significant and large changes in expression in at least one of the time-points/treatments compared to controls (|log2| >1.5, *P* < 0.05).

treatment persisted when a dendrogram was generated for the 931 gene expression changes found to be both significant (*P* < 0.05) and relatively large (|fold change| >1.5) (Fig. 2B), similar to what was observed in the TAMH model. The observation that significantly large changes in gene expression were consistently associated with drug treatment both *in vivo* and *in vitro* suggests that these highly differentially regulated transcripts can be used with high probability to delineate the toxicologic differences associated with APAP and AMAP treatments.

Expression of p53-related transcripts was consistently found to be differentially regulated in APAP treatment compared to AMAP treatments. In an attempt to identify transcripts with the most robust changes in expression, genes were identified where differential expression was seen at all time-points in the Affymetrix Mouse Genome 430 2.0 (|fold change| >2), Affymetrix Mouse Gene 1.0 ST (|fold change| >1.5, *P* < 0.05), and Agilent Mouse Oligonucleotide (|fold change| >1.5, *P* < 0.05) arrays (Fig. 3). Expression values for the 10 transcripts that were identified by multiple arrays as differentially expressed between the regioisomers (ie, shared Venn regions in Fig. 3) are listed in Table 1. In addition, differential expression values for transcripts exclusive to the Affymetrix Mouse Genome 430 2.0, Affymetrix Mouse Gene 1.0 ST, and Agilent Mouse Oligonucleotide arrays can be found in Supplementary Tables 1, 2, and 3, respectively. Strikingly, all 10 of the transcripts identified in common across the three arrays have published reports linking their activity to p53 signaling, suggesting that perturbations to p53 signaling pathways via differential transcriptomic regulation of p53-related factors are critical for promoting APAP-induced toxicity, AMAP-induced cytoprotection, or both. Interestingly, each dataset was mined retrospectively to assess the expression of *p53* itself, and no significant differences in its expression were observed at any time-point when comparing APAP and AMAP treatments.

APAP-induced expression of *Atf3*, *Btg2*, *Gdf15*, and *Jun* was the most consistent transcriptomic signature differentiating APAP and AMAP treatments. Of the 10 transcripts identified by multiple arrays, only *Atf3*, *Btg2*, *Gdf15*, and *Jun* were identified by all three array platforms as meeting significance and fold-change criteria at all time-points assayed (Table 1). Graphs were then constructed in order to track how gene expression changed for these transcripts over time for each platform (Fig. 4). *In vitro* expression of *Atf3*, *Btg2*, *Gdf15*, and *Jun* was relatively constant across all time-points (Fig. 4A and 4B), whereas *in vivo* expression of these four transcripts decreased after six hours (Fig. 4C). However, differential expression of *Atf3*, *Btg2*, *Gdf15*, and *Jun* was still maintained to a significant and large extent over all time-points in vivo despite decreased expression at later time-points (Table 1). It
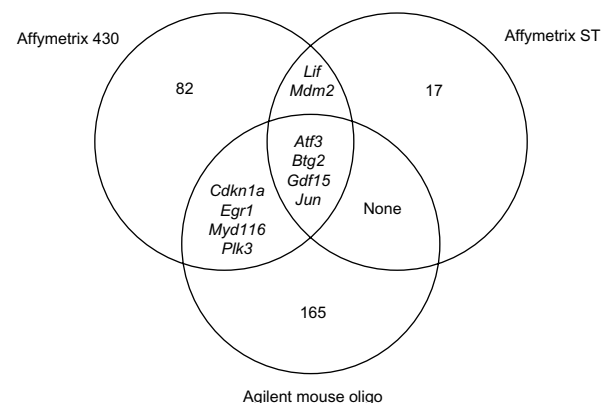
Figure 3. Transcripts differentially expressed at all time-points between APAP versus AMAP treatments. Venn diagrams represent the commonality and exclusivity of transcripts found to be differentially expressed in APAP relative to AMAP treated samples in the Affymetrix Mouse Genome 430 2.0 (|fold change| >2), Affymetrix Mouse Gene 1.0 ST (|fold change| >1.5, *P* < 0.05), and Agilent Mouse Oligonucleotide (|fold change| >1.5, *P* < 0.05) array data sets. Four transcripts were identified as shared across all three platforms: *Atf3*, *Btg2*, *Gdf15*, and *Jun*.

Table 1. Transcripts differentially expressed across multiple platforms at all time-points between APAP and AMAP treatments.

GENBANK ACCESSION	GENE SYMBOL	AFFY MOUSE GENOME 430 2.0 (FOLD CHANGE)			AFFY MOUSE GENE 1.0 ST (FOLD CHANGE)			AGILENT MOUSE OLIGONUCLEOTIDE (FOLD CHANGE)		
		APAP2_AMAP2	APAP6_AMAP6	APAP24_AMAP24	APAP2_AMAP2	APAP6_AMAP6	APAP24_AMAP24	APAP6_AMAP6	APAP12_AMAP12	APAP24_AMAP24
NM_007498	*Atf3*	4.8	16.1	17.0	**2.5**	**3.6**	**3.6**	**5.7**	**3.0**	**1.8**
NM_007570	*Btg2*	6.0	5.6	4.1	**2.2**	**2.0**	**2.3**	**6.4**	**2.9**	**2.4**
NM_007669	*Cdkn1a*	3.8	13.8	5.0	**1.5**	**2.2**	**3.1**	**2.7**	**2.2**	**2.5**
NM_007913	*Egr1*	5.8	3.0	3.5	**2.1**	**1.4**	**1.4**	**18.1**	**6.1**	**2.9**
NM_011819	*Gdf15*	12.5	15.7	9.1	**2.1**	**2.6**	**2.5**	**3.8**	**2.0**	**1.8**
NM_010591	*Jun*	4.3	3.1	4.5	**2.3**	**2.2**	**2.7**	**4.5**	**2.4**	**1.6**
NM_008501	*Lif*	4.6	5.1	4.5	**1.6**	**1.7**	**1.8**	N.S.[a]	0.8	0.8
NM_010786	*Mdm2*	4.0	5.2	2.9	**1.6**	**1.9**	**2.8**	1.3	1.2	1.2
NM_008654	*Myd116*	3.2	6.3	4.0	N.S.[a]	**1.8**	**2.2**	**2.2**	**1.9**	**1.7**
NM_013807	*Plk3*	3.8	3.0	3.1	**1.5**	**1.3**	**1.4**	**4.7**	**2.2**	**1.6**

Notes: Values in bold represent changes that were statistically significant ($P < 0.05$). [a]Not significant.

is also worth noting that differential expression of these four transcripts was also observed in the only other published toxicogenomic study comparing APAP and AMAP treatments.[16] In fact, differential expression of the numerous transcripts identified herein was also observed in the aforementioned toxicogenomic study (Table 2).

Protein expression of p53 following APAP and AMAP treatment in TAMH cells. An *in vitro* comparison was performed to assess p53 activity in two biologic replicates from TAMH cells dosed with 2 mM APAP or 2 mM AMAP at two and six hours. Western Blotting and subsequent densitometric analysis demonstrated that total p53 levels were marginally higher following APAP treatment than either control or AMAP treatments at both two- and six-hour time-points (Fig. 5). The greatest increase in total p53 expression was observed between the two-hour APAP and AMAP treatments (1.8-fold). In addition to total p53 measurements, p53 phosphorylation levels were also measured at two independent sites, S15 and S392. More than 4.4-fold increases in S15 phosphorylation were detected in APAP-treated samples for all time-matched comparisons (Fig. 6A). Similar results were observed at S392, in that APAP induced >5.8-fold increases in phosphorylation at this site compared to all other time-matched samples (Fig. 6B). The protein data strongly support the gene expression results by confirming that APAP-induced expression of p53-related transcripts is in fact accompanied by increased p53 phosphorylation.

Discussion

The goal of the present study was to identify a robust transcriptomic signature distinguishing the toxicologic differences between APAP and AMAP utilizing multiple model systems for APAP-induced toxicity across multiple microarray platforms. The two systems used in this study are well-characterized models for APAP-induced hepatotoxicity. The *in vitro* model (TAMH), an immortalized mouse hepatocyte line,[32] has been established as an acceptable cell culture model to study toxicologic differences between APAP and AMAP. This is due to the fact that TAMH express CYP2E1 and CYP3A proteins and show characteristic markers of APAP-mediated cell death processes that are accompanied by changes in cell morphology indicative of toxicity.[17,33] Results from the exploratory and follow-up TAMH microarray studies were then compared with those of a previously published comprehensive multi-center study that used C57BL/6J mice,[7] a well-characterized *in vivo* model for APAP-induced hepatocellular injury.[13,34,35]

Transcripts with significantly large differential expression at all time-points across all array platforms were identified in order to enrich for robust gene expression changes likely responsible for the differential toxicologic outcomes following APAP and AMAP treatment. Only four transcripts, *Atf3, Btg2, Gdf15*, and *Jun*, were identified (Fig. 3), and while APAP-induced upregulation of transcripts was consistent in both models at all assayed time-points, there was one obvious discrepancy between the *in vitro* and *in vivo* models. *In vitro* mRNA expression levels of *Atf3*, *Btg2*, *Gdf15*, and *Jun* were relatively constant across all time-points, whereas *in vivo* expression levels fell after six hours (Fig. 4). This discrepancy might be due to the high drug concentration throughout the dosing regimen *in vitro*, which could explain the persistence of large differential expression across all time-points. In contrast,
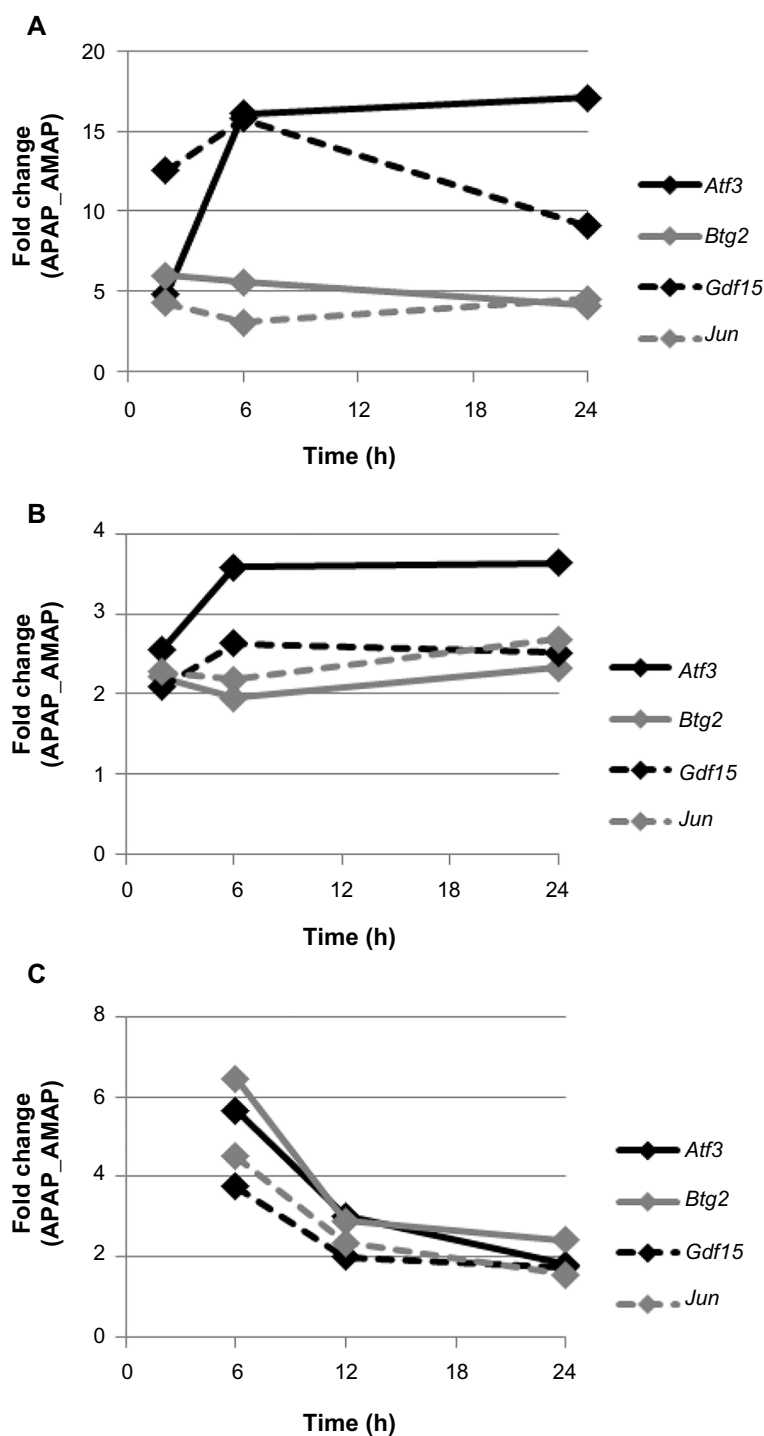
Figure 4. Time course of transcripts differentially expressed across all platforms at all time-points in the APAP versus AMAP comparison. Expression of *Atf3*, *Btg2*, *Gdf15*, and *Jun* are plotted versus time. *In vitro* measurements were taken at 2, 6, or 24 hours for the (**A**) Affymetrix Mouse Genome 430 2.0 and (**B**) Affymetrix Mouse Gene 1.0 ST arrays, whereas in vivo time-points for the (**C**) Agilent Mouse Oligonucleotide array were taken at 6, 12, or 24 hours.

mice have the ability to clear the drugs and their metabolites, which may explain the loss of differential expression over time *in vivo*.

APAP-induced upregulation of six additional transcripts (*Lif, Mdm2, Cdkn1a, Egr, Myd116*, and *Plk3*) were identified along with *Atf3, Btg2, Gdf15*, and *Jun* when the gene list was expanded to include transcripts where significantly large differential expression at all time-points across multiple platforms was observed (Table 1). These data are consistent with recent findings that hepatotoxicant exposure promotes upregulation of a consensus early response gene signature that includes *Egr1*, *Atf3*, and *Gdf15*.[36] An exhaustive literature search was then performed to identify a common pathway for the majority of these genes. Interestingly, not only

Table 2. Comparison of APAP- and AMAP-induced gene regulation consistent among multiple toxicogenomic studies between four and six hours of treatment.

GENE	AFFY MOUSE GENOME 430 2.0 (6 H)[a]	AFFY MOUSE GENE 1.0 ST (6 H)[b,7]	AGILENT MOUSE OLIGONUCLEOTIDE (6 H)[b,7]	CODELINK OLIGONUCLEOTIDE MOUSE UNISET 20K (6 H)[16]
	APAP_AMAP			
Atf3	↑	↑	↑	↑
Btg2	↑	↑	↑	↑
Cdkn1a	↑	↑	↑	
Cxcl10		↑	↑	↑
Cxcl2		↑		↑
Ddit3	↑	↑	↑	↑
Dnajb1 (Hsp40)			↑	↑
Egr1	↑		↑	
Gadd45a		↑	↑	↑
Gdf15	↑	↑	↑	↑
Hsph1 (Hsp105)			↑	↑
Jun	↑	↑	↑	↑
Myd116	↑	↑	↑	↑
Sprr1a	↑	↑		↑

Notes: [a]Fold change >2. [b]Fold change > 1.5, $P < 0.05$.

Figure 5. APAP- and AMAP-induced changes in total p53 protein levels. TAMH cells were treated with 2 mM APAP or AMAP for two and six hours. Total cell lysates were analyzed by western immunoblotting using a monoclonal anti-p53 antibody. Peaks represent quantified bands using ImageJ software, as described in the Materials and methods section.

could all 10 transcripts be linked to p53 signaling, but all 10 transcripts have been implicated in p53 signaling pathways (Fig. 7). p53 is an extraordinarily well-studied tumor suppressor that plays a key role in the cellular response to genotoxic stress.[19,37] Therefore, the identification of 10 transcripts unique to APAP treatment and associated with p53 would implicate a potential genotoxic mechanism in differentiating the toxicologic outcomes of APAP and AMAP. Proposed mechanisms by which the four transcripts identified in both models at all time-points across all three microarray platforms (*Atf3, Btg2, Gdf15*, and *Jun*) modulate p53 signaling can be found in Table 3, whereas the proposed mechanism by which the remaining six transcripts identified at all time-points across two microarray platforms (*Cdkn1a, Egr1, Lif, Mdm2, Myd116*, and *Plk3*) modulate p53 signaling can be found in Table 4.

Taken together, upregulation of these 10 transcripts, all of which are associated with p53 activity at all-time-points in multiple platforms, implicates a role for p53 in differentiating the toxicologic outcomes of APAP and AMAP (Fig. 7), especially considering that all these genes except for *Jun* and
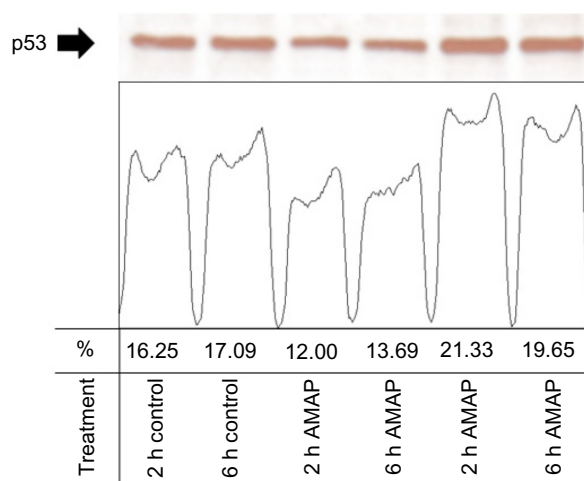
Myd116 have published reports of p53 response elements in their promoter regions.[38,39] Only two of the transcripts identified (*Jun* and *Mdm2*) are generally associated with negative p53 regulation. While these observations contradict the proposed model for p53-mediated APAP-induced toxicity, there have been reports of concomitant upregulation of *Jun* and *p53* during apoptosis.[40] JNK, an upstream kinase that phosphorylates Jun, also phosphorylates p53, leading to an increase in p53 stability, transcriptional activity, and apoptotic capacity.[41–43] APAP-induced JNK activation has not only been shown previously to potentiate APAP-induced hepatocellular injury[44–46] but also to distinguish toxicological differences between APAP and AMAP.[17] Likewise, the identification of *Mdm2* as a proposed mediator of APAP toxicity may appear counterintuitive since it is a known antagonist of p53 activity. At first glance, it would appear that high levels of *Mdm2* mRNA would equate to high Mdm2 protein levels and thus increased p53 degradation. However, the *Mdm2*–p53 interaction is not so straightforward. Negative regulation of p53 by *Mdm2* only occurs at the protein level, and many regulatory factors are capable of acting on Mdm2 to preserve p53 stability and stabilize function. Additionally, post-translational modifications to *Mdm2*, such as phosphorylation, have been shown to inhibit Mdm2-directed turnover of p53.[47] At the transcriptional level, p53 protein regulates *Mdm2* expression through a p53 DNA-binding site and a genetically responsive element demonstrating an *Mdm2*–p53 autoregulatory loop.[48]

The identification of these robust p53-related transcripts associated with APAP-induced toxicity is corroborated by other studies in which similar gene expression changes were observed in comparisons between APAP and AMAP treatments (Table 2). Numerous toxicogenomic studies in murine models investigating APAP-induced changes without AMAP
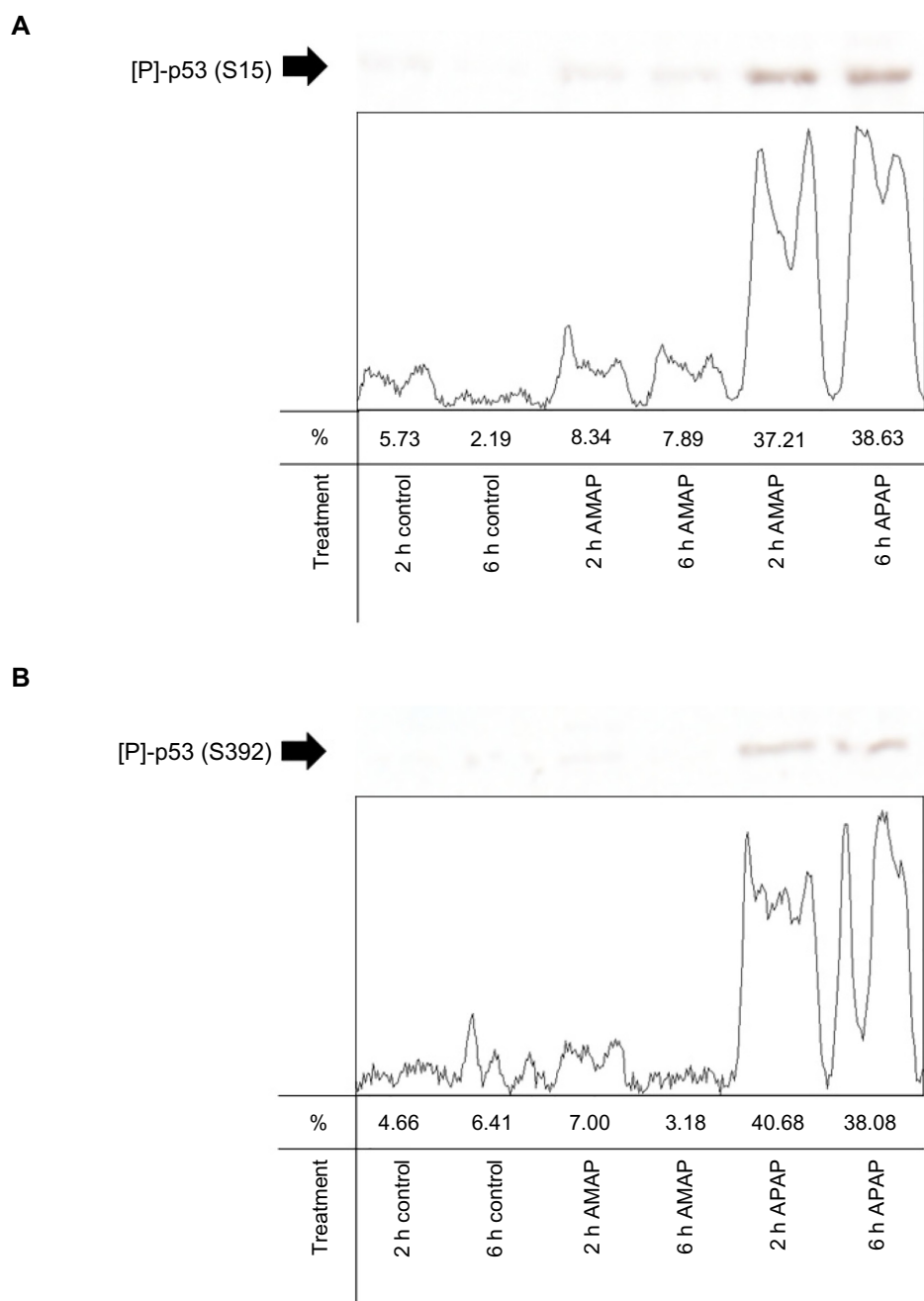
Figure 6. APAP- and AMAP-induced changes in phosphorylated p53 protein levels. TAMH cells were treated with 2 mM APAP or AMAP for two and six hours. Total cell lysates were analyzed by western immunoblotting with either (**A**) polyclonal anti-phospho-p53 (S15) or (**B**) polyclonal anti-phospho-p53 (S392) antibodies and quantified. Peaks represent quantified bands using ImageJ software, as described in the Materials and methods section.

treatment comparisons have also been performed over the past 15 years, many of which utilized biologic assays to phenotypically anchor the involvement of toxicologic mechanisms leading to hepatocellular injury (Table 5). Results from these studies have led to consistent identification of transcriptional biomarkers associated with exposure to toxicologically relevant concentrations of APAP.[49] In fact, 8 of the 14 genes listed in Table 2 have been corroborated by these studies (*Atf3, Ddit3, Dnajb1, Egr1, Gadd45a, Hsph1, Jun, Myd116*).[11–14]

While comparisons between the *in vitro* and the *in vivo* models provide consistent transcriptomic correlations across different platforms, emphasis should be placed on the key transcripts identified coupled with the p53 protein findings. There is some evidence implicating increased p53 protein levels following APAP treatment in murine liver,[50] which is consistent with the results presented here (Fig. 5). However, other studies in non-hepatic models have demonstrated that APAP-induced changes in p53 protein expression were cell-type-dependent across multiple breast cancer cell lines[51] or decreased in C6 glioma and LLC-PK1 cells.[22] In addition to the use of different model systems, the discrepancy between our results and those presented by Lee et al might
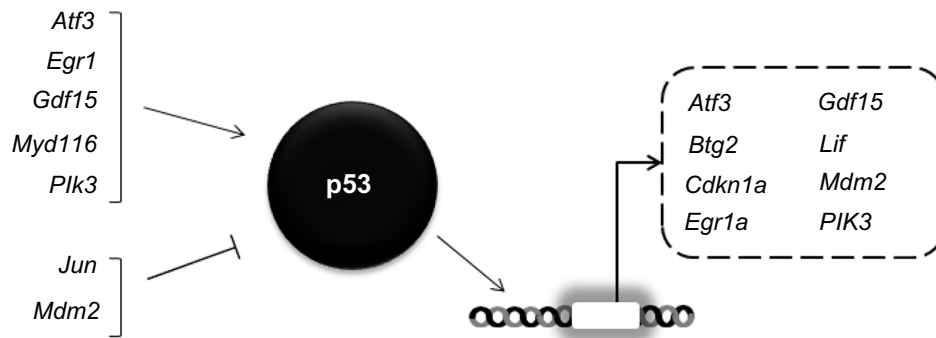
Figure 7. Differential expression of transcripts related to p53 signaling by APAP relative to AMAP treatment was consistently identified in both *in vitro* and *in vivo* models. Robust differential expression of the 10 genes associated with p53 signaling listed above (though not p53 itself) were identified following APAP and AMAP treatments at all time-points in multiple microarray platforms. *Atf3* and *Mdm2* are listed twice as they are known to act both upstream and downstream of p53 signaling.

Table 3. Transcripts identified in both models at all time-points across all three microarray platforms.

GENE	DESCRIPTION (ENTREZ GENE)	INTERACTIONS WITH p53 (REFERENCES)
Atf3	Stress-inducible ATF/CREB transcription factor family member	• Positively regulates p53 levels by increasing protein stability[65] • Functionally linked and directly activated by p53[66]
Btg2	BTG/Tob family member with anti-proliferative properties	• Promoter region contains a p53 response element[67] • Expression induced through a p53-dependent mechanism[68–70]
Gdf15	TGF-beta superfamily member that regulates tissue differentiation and maintenance	• Promoter region contains two p53-type response elements[71] • p53-dependent induction expression occurs in response to cell stress[72] • High levels can induce p53 activation as measured by p21 upregulation[73,74]
Jun	Transcription factor that interacts directly with specific target DNA sequences to regulate gene expression	• Represses p53 activity in multiple cell types: high p53 levels are observed when Jun is absent, and increased levels of Jun are thought to attenuate apoptosis by antagonizing p53 activity[75–77]

Table 4. Transcripts identified at all time-points across two microarray platforms.

GENE	DESCRIPTION (ENTREZ GENE)	INTERACTIONS WITH p53
Cdkn1a (p21)	Potent cyclin-dependent kinase inhibitor that regulates cell cycle progression	• *p21* promoter activity and protein expression are regulated in a p53-dependent manner[55,78]
Egr1	Nuclear protein that functions as a transcriptional regulator	• Acts both upstream and downstream of p53[39,79] • Directly interacts with p53, transactivates the p53 promoter, increases p53 RNA expression and protein levels, and regulates p53 protein stability[80–82] • Presumed gain-of-function p53 mutant leads to Egr1 upregulation through a physical association with the *Egr1* promoter[83] • All p53 family members are capable of inducing the Egr1 promoter[39]
Lif	Pleiotropic cytokine implicated in cell differentiation	• No studies investigating its interactions with p53 in hepatocytes; however, p53 regulates embryonic implantation through *Lif* transcriptional regulation, where loss of p53 results in decreases in both the level and function of Lif[84]
Mdm2	Nuclear phosphoprotein that binds and inhibits transactivation by p53	• Complexes with p53 and inhibits its transactivation by increasing p53 proteolysis by the 26S proteosome[85,86]
Myd116	Stress-induced murine homologue of the human *PPP1R15A* (*GADD34*) gene	• Induces p53 phosphorylation and subsequent activation resulting in growth arrest induction and apoptosis[55,87]
Plk3	Putative serine/threonine protein kinases that regulates cell cycle progression	• Induction occurs in a p53-dependent manner due to putative p53-response elements[88] • Complexes with and phosphorylates p53 inducing apoptosis[54,89,90]

be due to their use of a higher APAP dose (5 mM) or the use of dimethylsulfoxide (DMSO) as a vehicle control, which has been shown to alter p53 levels in some cell types.[52] However, it is worth noting that APAP did induce S15 phosphorylation in both TAMH (Fig. 6) and in C6 glioma cells,[22] which is associated with p53 regulation in response to cell stress signals.[53] Furthermore, the consistent upregulation of *Myd116* and *Plk3* transcripts observed in this study (Table 1) has been

Table 5. Gene expression studies investigating the effects of APAP exposure in murine models both *in vitro* and *in vivo*.

MODEL	APAP DOSE	TIME (H)	PLATFORM	DESCRIPTION
C57Bl/6 mice	300 mg/kg	6	Affymetrix Mu11K	Transcriptome profiling identified a wide array of differentially expressed gene sets[31]
Male C57Bl/6 mice	300 mg/kg	6	Affymetrix Mu11K	HSP expression is important in attenuating APAP-induced toxicity[11]
Male CD-1 mice	150, 500 mg/kg	0.25, 0.5, 1, 2, 4	AstraZeneca ToxBlot I	APAP-induced gene expression is useful in detecting cellular responses to acute toxic insult[12]
Female CD-1 mice	600 mg/kg	10	Atlas: customer-designed	Observed increased expression of genes related to cell stress, apoptosis, and DNA-damage[91]
Male AP-1 mice	50, 150, or 500 mg/kg	0.25, 0.5, 1, 2, 4	Affymetrix Mu11K	Observed decreased expression of genes involved in energy metabolism[92]
Male CD-1 mice	151, 529 mg/kg	1, 4, 24	Affymetrix U74v2	Characterized time- and dose-dependent expression of numerous APAP-responsive genes[14]
Male SJL mice; Male C57Bl/6 mice; Male F1 mice	300 mg/kg	3, 6, 12, 24	Affymetrix U74v2	Compared mouse strains with variable resistance to APAP-induced liver injury to identify DILD biomarkers[13]
Male C57Bl/6J mice[a]	300 mg/kg[b]	6, 12, 24	Agilent #G4121	Phenotypic anchoring is critical for obtaining meaningful toxicogenomic data across different experiments[7]
C57Bl/6 mice[a]	400 mg/kg[b]	6	CodeLink UniSet 20K	APAP-AMAP structure-toxicity relationship is capable of focusing transcriptome analysis to fewer genes of interest[16]
Male CD-1 mice	300 mg/kg	1.5, 4	Agilent #G4121	APAP alters IFN-β-mediated hepatic gene expression; however, few APAP alone led to few expression changes[93]
TAMH cell line[a]	2 mMb	2, 6	Affymetrix 1.0 ST	Upregulation of JNK-mediated transcription factors are important in propagating APAP-induced toxicity[17]
Male C57Bl/6J mice (and primary hepatocytes)	5, 50 or 500 mg/kg (0.1, 1, 10 mM)	8	Liver Stress Array v2	Isolated hepatocytes exposed to APAP underestimate the *in vivo* response[94]
Female C57Bl/6 mice	350 mg/kg	3, 8, 24, 48, 72	Agilent 4 × 44K	Discrepancies between live and plasma transcriptomes following APAP exposure[95]

Notes: [a]studies comparing APAP and AMAP structure-toxicity profiles. [b]equivalent AMAP dose administered.
Abbreviations: APAP, acetaminophen; AMAP, acetyl-*m*-aminophenol; DILD, drug-induced liver disease; IFN, interferon; JNK, c-Jun NH_2-terminal protein kinase.

associated with increased N-terminal p53 phosphorylation[54,55] and modulation of p53 stability and activity.[56,57]

In this study, APAP treatment also led to increased phosphorylation at S392 compared to AMAP and control (Fig. 6B). This is the first published evidence of dual p53 phosphorylation at both S15 and S392 in APAP-induced liver toxicity. *In vitro* studies have shown that S392 phosphorylation may prevent nuclear exportation of p53[58] and enhance p53 binding to sequence-specific DNA sites.[59] Increased dual phosphorylation of p53 at S15 and S392 following APAP treatment (Fig. 6) would suggest that not only is DNA damage occurring in response to cell stress (S15 phosphorylation) but p53-mediated transcriptional activity may also be enhanced due to an increase in nuclear stability of p53 (S392 phosphorylation). This proposed mechanism would explain the robust transcriptional response that was observed in p53-responsive genes across microarray platforms and model systems (Table 1). It also bears repeating that no differential expression of *p53* mRNA was observed following APAP and AMAP treatments in

any model across any time-point, suggesting that p53 activity as opposed to *p53* transcription is the driving force behind APAP-induced toxicity compared to AMAP. Coupled with the transcriptomic findings, the protein-based analysis further indicates a cellular stress response and implicates p53 as an important biological pathway involved in the response to tissue damage.

Lastly, it is important to discuss the relationship between oxidative stress and p53 signaling. In 2008, it was reported that *p21*, *Gdf15*, *Plk3*, *Atf3*, *Ddit4*, *Gadd45a*, *Btg2*, *Ndrg1*, and *Trp53inp1* were the genes most commonly upregulated in response to diquat-induced oxidative stress across three C57BL/6J mouse strains (wild-type, *Gpx1*^{−/−}, and *Sod*^{−/−}).[60] All nine of these oxidative-stress-responsive p53 target genes are predominantly involved in cell cycle arrest rather than apoptosis.[61] Of greater interest is the fact that five of these nine transcripts were identified in our analysis (Table 1). This consistency further supports a mechanism by which APAP, and not AMAP, exerts its toxicologic effects on cells

through p53-mediated processes induced by oxidative stress. Strong evidence already exists suggesting that APAP treatment generates oxidative stress and subsequent JNK activation in mice.[17,46,62] Additionally, the prolonged half-life of pro-oxidant APAP metabolites (ie, NAPQI), compared to the shorter-lived and more reactive pro-oxidant AMAP metabolites (ortho/para quinones), leads to greater dispersion of NAPQI throughout the cell (ie, mitochondrial damage), which may result in prolonged exposure to oxidative stress and thus potentiating p53-mediated processes.[63]

Conclusion

In conclusion, transcriptomic comparisons between APAP and AMAP using a well-characterized *in vitro* mouse model (TAMH) across two Affymetrix array platforms (Mouse Genome 430 2.0 and Mouse Gene 1.0 ST) with a well-characterized *in vivo* system (C57BL/6J mice) on an Agilent Oligonucleotide array[7] identified activation of p53 signaling as an important factor in APAP-induced toxicity at the transcriptional level. Furthermore, upregulation of the majority of the p53-related transcripts identified in this study are oxidative-stress-responsive, and their involvement in cell cycle arrest rather than apoptosis suggests that APAP-induced p53 signaling may contribute to the absence of apoptosis during APAP induced hepatocellular injury.[64] This APAP-induced transcriptional activation is related to increased phosphorylation at serine residues in both the N- and C- termini of p53. Along with the transcriptional data, the activity of p53 was analyzed, enabling us to place the transcriptional changes in the context of the wider biological response. By utilizing AMAP/APAP structure–toxicity relationships, this study demonstrated p53 signaling as a contributor to differentiating the toxicities of the regioisomers.

Acknowledgment

Author Contributions

Conceived and designed the experiments: BDS, MLG, DQN, FMF, SDN. Analyzed the data: BDS, MLG, DQN, RPB, TKB. Wrote the first draft of the manuscript: BDS. Contributed to the writing of the manuscript: BDS, MLG, DQN, TJK, SDN. Agree with manuscript results and conclusions: BDS, MLG, DQN, RPB, TKB, FMF, TJK, SDN. Jointly developed the structure and arguments for the paper: BDS, MLG. Made critical revisions and approved final version: BDS, MLG, TJK. All authors, with the exception of SDN, reviewed and approved of the final manuscript.

Supplementary Data

Supplementary Figure 1. is a dendrogram showing that gene expression changes cluster more closely with dosing period than by drug treatment. The dendrogram represents gene expression patterns for the 5753 genes with |fold change| >2 in at least one of the time-points/treatments relative to control in the Affymetrix Mouse Genome 430 2.0 array.

Supplementary Tables 1–3. provide differential expression values for transcripts exclusive to the Affymetrix Mouse Genome 430 2.0 (Supplementary Table 1), Affymetrix Mouse Gene 1.0 ST (Supplementary Table 2), and Agilent Mouse Oligonucleotide (Supplementary Table 3) arrays.

REFERENCES

1. Lee WM. Acetaminophen and the U.S. Acute Liver Failure Study Group: lowering the risks of hepatic failure. *Hepatology*. 2004;40(1):6–9.
2. Nourjah P, Ahmad SR, Karwoski C, Willy M. Estimates of acetaminophen (paracetomal)-associated overdoses in the United States. *Pharmacoepidemiol Drug Saf*. 2006;15(6):398–405.
3. Hinson JA, Roberts DW, James LP. Mechanisms of acetaminophen-induced liver necrosis. *Handb Exp Pharmacol*. 2010;196:369–405.
4. Pennie WD, Tugwood JD, Oliver GJ, Kimber I. The principles and practice of toxigenomics: applications and opportunities. *Toxicol Sci*. 2000;54(2):277–83.
5. Waring JF, Jolly RA, Ciurlionis R, et al. Clustering of hepatotoxins based on mechanism of toxicity using gene expression profiles. *Toxicol Appl Pharmacol*. 2001;175(1):28–42.
6. Bammler T, Beyer RP, Bhattacharya S, et al; Members of the Toxicogenomics Research Consortium. Standardizing global gene expression analysis between laboratories and across platforms. *Nat Methods*. 2005;2(5):351–6.
7. Beyer RP, Fry RC, Lasarev MR, et al; Members of the Toxicogenomics Research Consortium. Multicenter study of acetaminophen hepatotoxicity reveals the importance of biological endpoints in genomic analyses. *Toxicol Sci*. 2007;99(1):326–37.
8. Irizarry RA, Warren D, Spencer F, et al. Multiple-laboratory comparison of microarray platforms. *Nat Methods*. 2005;2(5):345–50.
9. Irwin RD, Boorman GA, Cunningham ML, Heinloth AN, Malarkey DE, Paules RS. Application of toxicogenomics to toxicology: basic concepts in the analysis of microarray data. *Toxicol Pathol*. 2004;32(suppl 1):72–83.
10. Jeong SY, Lim JS, Park HJ, Cho JW, Rana SV, Yoon S. Effects of acetaminophen on hepatic gene expression in mice. *Physiol Chem Phys Med NMR*. 2006;38(2):77–83.
11. Reilly TP, Bourdi M, Brady JN, et al. Expression profiling of acetaminophen liver toxicity in mice using microarray technology. *Biochem Biophys Res Commun*. 2001;282(1):321–8.
12. Ruepp SU, Tonge RP, Shaw J, Wallis N, Pognan F. Genomics and proteomics analysis of acetaminophen toxicity in mouse liver. *Toxicol Sci*. 2002;65(1):135–50.
13. Welch KD, Reilly TP, Bourdi M, et al. Genomic identification of potential risk factors during acetaminophen-induced liver disease in susceptible and resistant strains of mice. *Chem Res Toxicol*. 2006;19(2):223–33.
14. Williams DP, Garcia-Allan C, Hanton G, et al. Time course toxicogenomic profiles in CD-1 mice after nontoxic and nonlethal hepatotoxic paracetamol administration. *Chem Res Toxicol*. 2004;17(12):1551–61.
15. Nelson EB, Inventor; The Research Foundation of State University of New York, assignee. Method for analgesia using 3-hydroxyacetanilide. US patent 4,238,5081981. August 17, 1979.
16. Priyadarsiny P, Khattar SK, Malik R, et al. Differential gene expression analysis of a known hepatotoxin, N-acetyl-p-amino-phenol (APAP) as compared to its non-toxic analog, N-acetyl-m-amino-phenol (AMAP) in mouse liver. *J Toxicol Sci*. 2008;33(2):163–73.
17. Stamper BD, Bammler TK, Beyer RP, Farin FM, Nelson SD. Differential regulation of mitogen-activated protein kinase pathways by acetaminophen and its nonhepatotoxic regioisomer 3'-hydroxyacetanilide in TAMH cells. *Toxicol Sci*. 2010;116(1):164–73.
18. Waring JF, Ciurlionis R, Jolly RA, Heindel M, Ulrich RG. Microarray analysis of hepatotoxins in vitro reveals a correlation between gene expression profiles and mechanisms of toxicity. *Toxicol Lett*. 2001;120(1–3):359–68.
19. Levine AJ, Oren M. The first 30 years of p53: growing ever more complex. *Nat Rev Cancer*. 2009;9(10):749–58.
20. Toledo F, Wahl GM. Regulating the p53 pathway: in vitro hypotheses, in vivo veritas. *Nat Rev Cancer*. 2006;6(12):909–23.
21. McGill MR, Williams CD, Xie Y, Ramachandran A, Jaeschke H. Acetaminophen-induced liver injury in rats and mice: comparison of protein adducts, mitochondrial dysfunction, and oxidative stress in the mechanism of toxicity. *Toxicol Appl Pharmacol*. 2012;264(3):387–94.

22. Lee YS, Wan J, Kim BJ, Bae MA, Song BJ. Ubiquitin-dependent degradation of p53 protein despite phosphorylation at its N terminus by acetaminophen. *J Pharmacol Exp Ther.* 2006;317(1):202–8.

23. Wan J, Bae MA, Song BJ. Acetoaminophen-induced accumulation of 8-oxode-oxyguanosine through reduction of Ogg1 DNA repair enzyme in C6 glioma cells. *Exp Mol Med.* 2004;36(1):71–7.

24. Blaydes JP, Hupp TR. DNA damage triggers DRB-resistant phosphorylation of human p53 at the CK2 site. *Oncogene.* 1998;17(8):1045–52.

25. Kapoor M, Lozano G. Functional activation of p53 via phosphorylation following DNA damage by UV but not gamma radiation. *Proc Natl Acad Sci USA.* 1998;95(6):2834–7.

26. Lu H, Taya Y, Ikeda M, Levine AJ. Ultraviolet radiation, but not gamma radiation or etoposide-induced DNA damage, results in the phosphorylation of the murine p53 protein at serine−389. *Proc Natl Acad Sci U S A.* 1998;95(11):6399–402.

27. Gentleman RC, Carey VJ, Bates DM, et al. Bioconductor: open software development for computational biology and bioinformatics. *Genome Biol.* 2004;5(10):R80.

28. Smyth GK. Linear models and empirical bayes methods for assessing differential expression in microarray experiments. *Stat Appl Genet Mol Biol.* 2004;3:Article3.

29. Benjamini Y, Hochberg Y. Controlling the false discovery rate: a practical and powerful approach to multiple testing. *J Roy Stat Soc B Met.* 1995;57: 289–300.

30. Eaton SL, Roche SL, Llavero Hurtado M, et al. Total protein analysis as a reliable loading control for quantitative fluorescent western blotting. *PLoS One.* 2013;8(8):e72457.

31. Reilly TP, Brady JN, Marchick MR, et al. A protective role for cyclooxygenase-2 in drug-induced liver injury in mice. *Chem Res Toxicol.* 2001;14(12):1620–8.

32. Wu JC, Merlino G, Cveklova K, Mosinger B Jr, Fausto N. Autonomous growth in serum-free medium and production of hepatocellular carcinomas by differentiated hepatocyte lines that overexpress transforming growth factor alpha 1. *Cancer Res.* 1994;54(22):5964–73.

33. Pierce RH, Franklin CC, Campbell JS, et al. Cell culture model for acetaminophen-induced hepatocyte death in vivo. *Biochem Pharmacol.* 2002;64(3): 413–24.

34. Aleksunes LM, Campion SN, Goedken MJ, Manautou JE. Acquired resistance to acetaminophen hepatotoxicity is associated with induction of multidrug resistance-associated protein 4 (Mrp4) in proliferating hepatocytes. *Toxicol Sci.* 2008;104(2):261–73.

35. Martinez SM, Bradford BU, Soldatow VY, et al. Evaluation of an in vitro toxicogenetic mouse model for hepatotoxicity. *Toxicol Appl Pharmacol.* 2010;249(3):208–16.

36. Zhang JD, Berntenis N, Roth A, Ebeling M. Data mining reveals a network of early-response genes as a consensus signature of drug-induced in vitro and in vivo toxicity. *Pharmacogenomics J.* 2014;14:208–16.

37. Burns TF, El-Deiry WS. The p53 pathway and apoptosis. *J Cell Physiol.* 1999;181(2):231–9.

38. Riley T, Sontag E, Chen P, Levine A. Transcriptional control of human p53-regulated genes. *Nat Rev Mol Cell Biol.* 2008;9(5):402–12.

39. Yu J, Baron V, Mercola D, Mustelin T, Adamson ED. A network of p73, p53 and Egr1 is required for efficient apoptosis in tumor cells. *Cell Death Differ.* 2007;14(3):436–46.

40. Nango R, Terada C, Tsukamoto I. Jun N-terminal kinase activation and upregulation of p53 and p21(WAF1/CIP1) in selenite-induced apoptosis of regenerating liver. *Eur J Pharmacol.* 2003;471(1):1–8.

41. Fuchs SY, Adler V, Pincus MR, Ronai Z. MEKK1/JNK signaling stabilizes and activates p53. *Proc Natl Acad Sci U S A.* 1998;95(18):10541–6.

42. Kobayashi K, Tsukamoto I. Prolonged Jun N-terminal kinase (JNK) activation and the upregulation of p53 and p21(WAF1/CIP1) preceded apoptosis in hepatocytes after partial hepatectomy and cisplatin. *Biochim Biophys Acta.* 2001;1537(1):79–88.

43. Milne DM, Campbell LE, Campbell DG, Meek DW. p53 is phosphorylated in vitro and in vivo by an ultraviolet radiation-induced protein kinase characteristic of the c-Jun kinase, JNK1. *J Biol Chem.* 1995;270(10):5511–8.

44. Gunawan BK, Liu ZX, Han D, Hanawa N, Gaarde WA, Kaplowitz N. c-Jun N-terminal kinase plays a major role in murine acetaminophen hepatotoxicity. *Gastroenterology.* 2006;131(1):165–78.

45. Hanawa N, Shinohara M, Saberi B, Gaarde WA, Han D, Kaplowitz N. Role of JNK translocation to mitochondria leading to inhibition of mitochondria bioenergetics in acetaminophen-induced liver injury. *J Biol Chem.* 2008;283(20):13565–77.

46. Saito C, Lemasters JJ, Jaeschke H. c-Jun N-terminal kinase modulates oxidant stress and peroxynitrite formation independent of inducible nitric oxide synthase in acetaminophen hepatotoxicity. *Toxicol Appl Pharmacol.* 2010;246(1–2): 8–17.

47. Deisenroth C, Zhang Y. Ribosome biogenesis surveillance: probing the ribosomal protein-Mdm2-p53 pathway. *Oncogene.* 2010;29(30):4253–60.

48. Wu X, Bayle JH, Olson D, Levine AJ. The p53-mdm-2 autoregulatory feedback loop. *Genes Dev.* 1993;7(7 A):1126–32.

49. Stamper BD. Transcriptional profiling of reactive metabolites for elucidating toxicological mechanisms: a case study of quinoneimine-forming agents. *Drug Metab Rev.* 2014;1–11. http://www.ncbi.nlm.nih.gov/pubmed/25351209

50. Ray SD, Balasubramanian G, Bagchi D, Reddy CS. Ca(2+)-calmodulin antagonist chlorpromazine and poly(ADP-ribose) polymerase modulators 4-aminobenzamide and nicotinamide influence hepatic expression of BCL-XL and P53 and protect against acetaminophen-induced programmed and unprogrammed cell death in mice. *Free Radic Biol Med.* 2001;31(3):277–91.

51. Gadd SL, Hobbs G, Miller MR. Acetaminophen-induced proliferation of estrogen-responsive breast cancer cells is associated with increases in c-myc RNA expression and NF-kappaB activity. *Toxicol Sci.* 2002;66(2):233–43.

52. Koiri RK, Trigun SK. Dimethyl sulfoxide activates tumor necrosis factoralpha-p53 mediated apoptosis and down regulates D-fructose-6-phosphate-2-kinase and lactate dehydrogenase-5 in Dalton's lymphoma in vivo. *Leuk Res.* 2011;35(7):950–6.

53. Appella E, Anderson CW. Post-translational modifications and activation of p53 by genotoxic stresses. *Eur J Biochem.* 2001;268(10):2764–72.

54. Xie S, Wu H, Wang Q, et al. Plk3 functionally links DNA damage to cell cycle arrest and apoptosis at least in part via the p53 pathway. *J Biol Chem.* 2001;276(46):43305–12.

55. Yagi A, Hasegawa Y, Xiao H, et al. GADD34 induces p53 phosphorylation and p21/WAF1 transcription. *J Cell Biochem.* 2003;90(6):1242–9.

56. Ashcroft M, Kubbutat MH, Vousden KH. Regulation of p53 function and stability by phosphorylation. *Mol Cell Biol.* 1999;19(3):1751–8.

57. Lambert PF, Kashanchi F, Radonovich MF, Shiekhattar R, Brady JN. Phosphorylation of p53 serine 15 increases interaction with CBP. *J Biol Chem.* 1998;273(49):33048–53.

58. Kim YY, Park BJ, Kim DJ, et al. Modification of serine 392 is a critical event in the regulation of p53 nuclear export and stability. *FEBS Lett.* 2004;572(1–3):92–8.

59. Hupp TR, Meek DW, Midgley CA, Lane DP. Regulation of the specific DNA binding function of p53. *Cell.* 1992;71(5):875–86.

60. Han ES, Muller FL, Pérez VI, et al. The in vivo gene expression signature of oxidative stress. *Physiol Genomics.* 2008;34(1):112–26.

61. Yu J, Zhang L. The transcriptional targets of p53 in apoptosis control. *Biochem Biophys Res Commun.* 2005;331(3):851–8.

62. Nakagawa H, Maeda S, Hikiba Y, et al. Deletion of apoptosis signal-regulating kinase 1 attenuates acetaminophen-induced liver injury by inhibiting c-Jun N-terminal kinase activation. *Gastroenterology.* 2008;135(4):1311–21.

63. Holme JA, Hongslo JK, Bjorge C, Nelson SD. Comparative cytotoxic effects of acetaminophen (N-acetyl-p-aminophenol), a non-hepatotoxic regioisomer acetyl-m-aminophenol and their postulated reactive hydroquinone and quinone metabolites in monolayer cultures of mouse hepatocytes. *Biochem Pharmacol.* 1991;42(5):1137–42.

64. Gujral JS, Knight TR, Farhood A, Bajt ML, Jaeschke H. Mode of cell death after acetaminophen overdose in mice: apoptosis or oncotic necrosis? *Toxicol Sci.* 2002;67(2):322–8.

65. Yan C, Lu D, Hai T, Boyd DD. Activating transcription factor 3, a stress sensor, activates p53 by blocking its ubiquitination. *EMBO J.* 2005;24(13):2425–35.

66. Zhang C, Gao C, Kawauchi J, Hashimoto Y, Tsuchida N, Kitajima S. Transcriptional activation of the human stress-inducible transcriptional repressor ATF3 gene promoter by p53. *Biochem Biophys Res Commun.* 2002;297(5):1302–10.

67. Duriez C, Falette N, Audoynaud C, et al. The human BTG2/TIS21/PC3 gene: genomic structure, transcriptional regulation and evaluation as a candidate tumor suppressor gene. *Gene.* 2002;282(1–2):207–14.

68. Boiko AD, Porteous S, Razorenova OV, Krivokrysenko VI, Williams BR, Gudkov AV. A systematic search for downstream mediators of tumor suppressor function of p53 reveals a major role of BTG2 in suppression of Ras-induced transformation. *Genes Dev.* 2006;20(2):236–52.

69. Kannan K, Amariglio N, Rechavi G, et al. DNA microarrays identification of primary and secondary target genes regulated by p53. *Oncogene.* 2001;20(18):2225–34.

70. Rouault JP, Falette N, Guéhenneux F, et al. Identification of BTG2, an antiproliferative p53-dependent component of the DNA damage cellular response pathway. *Nat Genet.* 1996;14(4):482–6.

71. Osada M, Park HL, Park MJ, et al. A p53-type response element in the GDF15 promoter confers high specificity for p53 activation. *Biochem Biophys Res Commun.* 2007;354(4):913–8.

72. Kelly JA, Lucia MS, Lambert JR. p53 controls prostate-derived factor/macrophage inhibitory cytokine/NSAID-activated gene expression in response to cell density, DNA damage and hypoxia through diverse mechanisms. *Cancer Lett.* 2009;277(1):38–47.

73. Abd El-Aziz SH, Endo Y, Miyamaori H, Takino T, Sato H. Cleavage of growth differentiation factor 15 (GDF15) by membrane type 1-matrix metalloproteinase abrogates GDF15-mediated suppression of tumor cell growth. *Cancer Sci.* 2007;98(9):1330–5.

74. Yang H, Filipovic Z, Brown D, Breit SN, Vassilev LT. Macrophage inhibitory cytokine-1: a novel biomarker for p53 pathway activation. *Mol Cancer Ther.* 2003;2(10):1023–9.

75. Eferl R, Ricci R, Kenner L, et al. Liver tumor development. c-Jun antagonizes the proapoptotic activity of p53. *Cell*. 2003;112(2):181–92.

76. Schreiber M, Kolbus A, Piu F, et al. Control of cell cycle progression by c-Jun is p53 dependent. *Genes Dev*. 1999;13(5):607–19.

77. Stepniak E, Ricci R, Eferl R, et al. c-Jun/AP-1 controls liver regeneration by repressing p53/p21 and p38 MAPK activity. *Genes Dev*. 2006;20(16):2306–14.

78. He G, Siddik ZH, Huang Z, et al. Induction of p21 by p53 following DNA damage inhibits both Cdk4 and Cdk2 activities. *Oncogene*. 2005;24(18):2929–43.

79. Krones-Herzig A, Adamson E, Mercola D. Early growth response 1 protein, an upstream gatekeeper of the p53 tumor suppressor, controls replicative senescence. *Proc Natl Acad Sci U S A*. 2003;100(6):3233–8.

80. Das A, Chendil D, Dey S, et al. Ionizing radiation down-regulates p53 protein in primary Egr-1-/- mouse embryonic fibroblast cells causing enhanced resistance to apoptosis. *J Biol Chem*. 2001;276(5):3279–86.

81. Liu J, Grogan L, Nau MM, Allegra CJ, Chu E, Wright JJ. Physical interaction between p53 and primary response gene Egr–1. *Int J Oncol*. 2001;18(4):863–70.

82. Nair P, Muthukkumar S, Sells SF, Han SS, Sukhatme VP, Rangnekar VM. Early growth response-1-dependent apoptosis is mediated by p53. *J Biol Chem*. 1997;272(32):20131–8.

83. Weisz L, Zalcenstein A, Stambolsky P, et al. Transactivation of the EGR1 gene contributes to mutant p53 gain of function. *Cancer Res*. 2004;64(22):8318–27.

84. Hu W, Feng Z, Teresky AK, Levine AJ. p53 regulates maternal reproduction through LIF. *Nature*. 2007;450(7170):721–4.

85. Momand J, Wu HH, Dasgupta G. MDM2 – master regulator of the p53 tumor suppressor protein. *Gene*. 2000;242(1–2):15–29.

86. Momand J, Zambetti GP, Olson DC, George D, Levine AJ. The mdm-2 oncogene product forms a complex with the p53 protein and inhibits p53-mediated transactivation. *Cell*. 1992;69(7):1237–45.

87. Haneda M, Kojima E, Nishikimi A, Hasegawa T, Nakashima I, Isobe K. Protein phosphatase 1, but not protein phosphatase 2 A, dephosphorylates DNA-damaging stress-induced phospho-serine 15 of p53. *FEBS Lett*. 2004;567(2–3):171–4.

88. Staib F, Robles AI, Varticovski L, et al. The p53 tumor suppressor network is a key responder to microenvironmental components of chronic inflammatory stress. *Cancer Res*. 2005;65(22):10255–64.

89. Bahassi el M, Conn CW, Myer DL, et al. Mammalian polo-like kinase 3 (Plk3) is a multifunctional protein involved in stress response pathways. *Oncogene*. 2002;21(43):6633–40.

90. Li Z, Niu J, Uwagawa T, Peng B, Chiao PJ. Function of polo-like kinase 3 in NF-kappaB-mediated proapoptotic response. *J Biol Chem*. 2005;280(17):16843–50.

91. Liu J, Li C, Waalkes MP, et al. The nitric oxide donor, V-PYRRO/NO, protects against acetaminophen-induced hepatotoxicity in mice. *Hepatology*. 2003;37(2):324–33.

92. Coen M, Ruepp SU, Lindon JC, et al. Integrated application of transcriptomics and metabonomics yields new insight into the toxicity due to paracetamol in the mouse. *J Pharm Biomed Anal*. 2004;35(1):93–105.

93. Farnsworth A, Flaman AS, Prasad SS, et al. Acetaminophen modulates the transcriptional response to recombinant interferon-beta. *PLoS One*. 2010;5(6):e11031.

94. Tachibana S, Shimomura A, Inadera H. Toxicity monitoring with primary cultured hepatocytes underestimates the acetaminophen-induced inflammatory responses of the mouse liver. *Tohoku J Exp Med*. 2011;225(4):263–72.

95. Wang K, Yuan Y, Li H, et al. The spectrum of circulating RNA: a window into systems toxicology. *Toxicol Sci*. 2013;132(2):478–92.